# Reanalysis of double EphA3 knockin maps in mouse shows the importance of chemoaffinity in topographic map formation

*David J Willshaw[1*] and Nicholas M Gale[2]*

## Summary

Double visual maps in the EphA3 knockin mouse have been used extensively to investigate the mechanisms for the formation of ordered nerve connections. Here, EphA3+ and EphA3- retinal ganglion cells, forming a mosaic, each make a separate map on the superior colliculus. We constructed ordered 2D maps from EphA3 knockin Fourier-based intrinsic imaging data. Over both EphA3+/- and EphA3+/+ genotypes, the extent and location in the visual field of each projection of a double map vary considerably. Aided by computer modelling results, we suggest that all EphA3 knockin maps are examples of a single type, with the amount of EphA3 in EphA3+ retinal cells varying between animals. Previous analysis of the same dataset suggested that EphA3+/- maps represent an unstable transition between single (wild type) and double (EphA3+/+) maps, reflecting a balance between molecular and electrical signalling. In contrast, our analysis highlights the importance of molecular-based cues in establishing the retinotopic map.

**Keywords:** topographic map formation, double maps, mouse, superior colliculus, EphA3 knockin, chemoaffinity, Fourier-based imaging, Lattice Method, anatomical-functional relationship, computer modelling.

## Introduction

In mammals, retinal ganglion cells develop an ordered map of nerve connections across the superior colliculus (Drager and Hubel, 1976; Finlay et al., 1978; King et al., 1996), thought to be a result of both chemical and electrical signalling (Pfeiffenberger et al, 2006; Cang and Feldheim, 2013)**.** In particular, the mapping of nasotemporal retina to rostrocaudal colliculus involves the EphA receptor tyrosine kinases and their ligands, the ephrinAs, distributed as gradients across the nasotemporal axis of the retina and the rostrocaudal axis of the colliculus respectively. Correspondingly, the mapping of dorsoventral retina to mediolateral colliculus is mediated by gradients of EphB running dorsoventrally and ephrinB running mediolaterally (Flanagan and Vanderhaeghen, 1998; McLaughlin et al., 2003a).
In an EphA3 knockin mouse, the EphA3 ligand, not normally present in mouse retina, becomes bound to the Islet2 class of retinal ganglion cells. These are distributed over the retina, in equal proportions in a salt-and-pepper fashion (Brown et al., 2000)**.** Using fibre tracing, Brown et al. (2000) showed that in a wildtype (WT) map there is a single ordered

[1]Institute for Adaptive and Neural Computation, School of Informatics, University of Edinburgh, 10 Crichton Street, Edinburgh, EH8 9AB, UK
[*]Correspondence: willshaw@inf.ed.ac.uk
[2]Department of Applied Mathematics and Theoretical Physics, University of Cambridge, Wilberforce Road, Cambridge CB3 0WA, UK

projection of the nasotemporal axis of the retina onto the rostrocaudal axis of the colliculus (Figure 1A). In the homozygous knockin (EphA3+/+) map (Figure 1C), the EphA3+ retinal cells are projected in order onto rostral colliculus, with a similar ordered projection from EphA3- cells more caudally, to form a double representation of visual field on colliculus. In the heterogenous knockin (EphA3+/-) map (Figure 1B), the two types of cells also project separately except that the projections coincide in far rostral colliculus (Figure 1B; Brown et al., 2000; Reber et al., 2004; Bevins et al., 2011).

It was suggested that in these neuroanatomical maps, the degree of separation of the two projections on the colliculus depends on the extra amount of EphA assigned to EphA3+ cells, in the homozygous knockins being double that in the heterozygous knockins**.** (Brown et al, 2000; Reber et al., 2004). These authors also suggested that in heterozygous knockins the relatively small difference in EphA between EphA3- and EphA3+ cells in temporal retina compared with the high level of endogenous EphA is not sufficient to separate the projections on rostral colliculus.

Owens et al. (2015) explored the EphA3+ knockin visuocollicular map using Fourier-based intrinsic imaging, where the visual field is scanned over two orthogonal directions. (Kalatsky and Stryker, 2003). They reported single projections in wildtypes and double projections in the EphA3+/+ knockins. In different EphA3+/- knockins they found both single, double and a mixture of single and double projections. Taken together with other experimental evidence and modelling results, they proposed that this variety amongst EphA3+/- knockins is due to a fine balance between activity-based forces favouring single maps and chemically-based forces favouring double maps; the mixed type of map represents an unstable state which can be converted into either a single or double map by small fluctuations in the two forces pitted against each other.

Since Owens et al. (2015) characterised their maps from sample rostrocaudal projections taken from one direction of scan, we decided to construct 2D maps using all the information available. We excluded information from regions of the colliculus where the signal strength was low, an indicator of noise (Kalatsky and Stryker, 2003; Cang et al., 2008) or where two unknown positions in the visual field mapped to the same area**.** Using the filtered information, we employed a novel method (Willshaw et al., 2014) to reconstruct the 2D visuocollicular map. This map represents the projection from colliculus to visual field and so there is no information available about the pattern of innervation from the EphA3+/+ or the EphA3+/- population separately. To help infer the map from visual field to colliculus, and thus the contribution to the map from these two classes of cells, we used simulation results from computer models (Triplett et al., 2011; Hjorth et al., 2015) where such information is available.

Constructing 2D maps might help decide whether the difference between the finding in EphA3+/- animals of a single type of anatomical map (Brown et al., 2000; Reber et al., 2004) against a variety of functional maps (Owens et al., 2015) is due to the differences between the experimental techniques. Fourier intrinsic imaging allows the map in a single animal to be reconstructed whereas anatomical maps are constructed from different animals, and so any heterogeneity may be averaged out.

## Results

The dataset is from 24 mice, five wildtypes (WT), five homozygous EphA3+ knockins (HOM) and 16 heterozygous EphA3+ knockins (HET) (Owens et al., 2015).

### *1D analysis: sampling the nasotemporal to rostrocaudal projection.*

Figures 1G-1R shows twelve examples of 1D maps of the projection from colliculus (row 2) to visual field (row 1). Information from the grey (eligible) pixels was used to construct the map after the green pixels were rejected by filtering. In WTs (Figures 1G, 1H) there is one large area of eligible pixels in the colliculus (row 2), taken to be the main projection area, surrounded by rejected pixels. In Figure 1H there is a small secondary projection area, seen also in Figure 2J. Heterozygous EphA3 knockins (HET; Figures 1I-1N) show a variety of projection areas. In some cases, there is one area of eligible pixels (Figures 1I,1J); in others there are signs of two projection areas with rejected pixels between them of various forms (Figures 1K-1N). Homozygous EphA3 knockins (HOM), show a clear separation of the colliculus into two projection areas (Figures 1O, 1P). Three cases (e.g., Figures 1Q, 1R) with highly abnormal 1D profiles did not show well-defined projection areas and were not analysed further.

Owens et al. (2015) took their three 1D visuocollicular profiles along three straight line tracks drawn on the colliculus (row 2, black dotted lines). These were intended to represent the projection at three standard elevations in the visual field. Our method was to draw three coloured straight lines on the colliculus by computing the straight line fit to all the points associated with the given elevation. We then projected each line of points back into the visual field. The projections in the visual field (row 1) are not perfectly aligned with the appropriate elevations, suggesting that the nasotemporal and dorsoventral aspects of the map cannot be separated easily.

Most of the 13 cases analysed each had a strong 1D map, extending from nasal field to cover most of the visual field (rows 3-5). In some of the profiles the map was absent or did not cover all of visual field (Figures 1G, 1I, row 5; Figures 1L, 1M, row 3), or had breaks in it (Figure 1K, rows 3,5; Figures 1L, 1N, row 4) In both the HOMs and the HETs, there was also a second projection from caudal colliculus of varying sizes, which was restricted to temporal field (Figures 1M-1O), rows 3-5 except Figure 1N, row 5). There were also other types of projection such as the small projection to temporal field from rostral colliculus (Figures 1H, 1J, rows 3-5).

In summary, many of the 1D projections are noisy. Viewing how the tracks along which the 1D profiles were taken run over the irregular regions of eligible pixels on the colliculus (row 2) suggests that the 1D profiles reconstructed are sensitive to the exact positioning of the tracks. We concluded that assessing the projection at three standard positions does not allow for the variability in the maps and the nature of the projections is more complex than a binary classification into single or double projections. Therefore, the 1D method of analysis was not pursued and 2D maps were constructed. This involves investigating how a lattice of representative points (nodes) drawn on the colliculus projects into the set of corresponding points in the visual field, as described in the Methods.

### *Wildtype (WT) maps*

To establish a base line, the five WTs in the dataset were analysed. In each case there is a single large and extremely well-ordered projection, including two with a small aberrant projection.

Figure 2A shows the complete projection between each of the nodes on the colliculus (bottom) to the matching nodes in the visual field (top) for the WT shown in Figure 1G. The red links, mainly in temporodorsal field and caudomedial colliculus, indicate regions where links in the field cross, indicating violation of neighbourhood relations. By removal of selected nodes, these links were removed until the largest ordered submap with perfect local order remained (Figure 2B). To give a sense of the overall polarity of the map and to relate these maps to the 1D slices shown in Figure 1G, three lines running nasotemporally which link the visual field nodes closest to the same standard elevations used in the 1D analysis were projected onto the colliculus. The map in Figure 2B has high local order with Map Quality, the percentage number of nodes in the largest ordered submap, of 96%. The rostrocaudal (RC) and mediolateral (ML) polarities, defined in Methods, are in excess of 90%.

Figures 2D-2F show another WT map with a strip of rejected pixels separating a large area of eligible pixels from a small area (Figure 1H). In the whole map (Figure 2D) there are many violations of neighbour relations. By dividing the collicular nodes into two with a line drawn through the strip of green rejected pixels and then constructing separate maps on the two collicular lattices so formed (Figures 2E, 2F), the small projection area rostrally was found to be associated with temporal field (Figure 2E). The massive violation of neighbour relationships seen in Figure 2D is due to a small part of temporal field being represented both rostrally and caudally.

In the group of five WTs, the number of nodes on the colliculus is 188±38, spanning an approximately 1 $mm^2$ circular region. Map Quality is 91±4% and the RC and ML polarities are 90±4% and 91±3%. The map is slightly more elongated along the (rotated) rostrocaudal axis than the (rotated) mediolateral axis. Azimuthal (AM) and Elevational magnifications (EM) are 93±13$^o$/mm, 71±9$^o$/mm).

*Heterozygous EphA3 knockin maps (HETS)*
Two datasets were discarded at the 1D analysis stage, one of these shown in Figure 1Q**.** The remaining 14 cases fall into three groups.

*HETA (5 cases).* In this group there is one projection area on the colliculus and a single ordered map. The largest ordered submap of one example is shown in Figure 2C, with pixel distributions in Figure 1I. These five maps are slightly less well-ordered than WTs, with Map Quality 86±2% against 91±4%. The number of nodes (190±22 against 188±38), the RC and ML polarity scores (91±2%; 90±1% against 91±4%; 91±3%) and the magnifications (98±16$^o$/mm, 63±5$^o$/mm against 93±13 $^o$/mm, 71±9$^o$/mm) are very similar to those in WTs (Figures 8A-8F).
In three cases, a small part of nasal field is associated with far caudal colliculus, pixel distribution shown in Figure 1J. These maps are similar to those found in two WTs, one illustrated in Figure 2D-2F. This might be caused by a misalignment during initial processing of the phase of the Fourier signal with the starting position of the azimuthal scan.

*HETB (4 cases)*
The two regions of eligible (grey) pixels on the colliculus suggest two incompletely separated projection areas with rejected pixels (green) interposed (Figures 1K,1L). These could represent noise or regions associated with two distinct areas of visual field and thus cannot be mapped. Figure 3 shows the maps for these two HETs. The rostral and caudal projection areas were defined by drawing a line through the narrow neck of the composite region. This enabled separate largest ordered sub-partmaps to be constructed on the rostral and caudal subdivisions of the colliculus (Figures 3B-3C, 3E-3F)**.** In both cases, total Map Quality is 3% more than in the single map.

In this category, the two separate partmaps make up a single map with only a very small area of visual field represented on both rostral and caudal subdivisions of the colliculus, the extent measured by the Visual Field Overlap (VFO). The area of visual field associated with rostral colliculus is 74±17% of the total occupied by the largest ordered submap against 30±15% to caudal colliculus, giving a VFO of 4±3%. Defining the total collicular region as the areas occupied by the rostral and caudal regions together with the area between them, the rostral region occupies 48±13% of the colliculus, the caudal region 33±10% and the central region 19±10%.

Map Quality of the two partmaps is 93±4% compared with 91±5% for the whole map, identical to the figure for WTs. The RC and ML polarities in both the largest ordered single sub-partmap and the largest ordered sub-partmap in rostral colliculus are all in excess of 90%, at the WT level, whereas for the smaller projection to caudal colliculus the figures are slightly lower (Figures 8C, 8D).

HETC (5 cases). The maps are well ordered with polarity scores and Map Quality greater than for the whole map (Figure 8A). There are strong indications of two projection areas. 91±11% of the visual field is represented in rostral colliculus and 27±14% in caudal colliculus giving larger VFOs than for HETBs, of 18±7%. Two HETCs, corresponding to Figures 1M, 1N, are shown in Figure 4. In both cases, whereas the projection from the rostral area is to the entire visual field (Figures 4B, 4E), there is no projection to visual field from the caudal area (Figures 4C, 4F), resulting in a higher AM than EM and significant VFO of 27% and 24% respectively (Figures 8E,8F, 8B). The averages sizes of the rostral region of projection, the caudal region and the central region are all similar.

### *Homozygote EphA3 knockin (HOM) maps*

Four of the five available data sets were analysed, the fifth being rejected as a result of the 1D analysis (Figure 1Q). In these four HOMs, partitioning the colliculus into two yields two distinct, well ordered partmaps. They have high polarity scores and Map Quality is 89±10%, substantially more than for the whole projection (Figure 8A). The rostral projection area has a projection from almost all (98±4%) of the visual field whereas the caudal region has a projection from about one third (35±20%), in temporal field. As a result, the VFO is substantial, varying widely with individual scores of 17%, 25%, 29% and 59% of the visual field, an average of 33±18*%.* The sizes of the rostral projection area, the caudal projection area and the area between them are very similar (32±10%, 32±13%. 35±7%). The fact that a larger area of visual field is associated with the rostral area than with the caudal area of the same size is reflected in the fact that the azimuthal magnification (AM) for the rostral partmap is double that for the caudal map: 203±20$^{o}$/mm against 101±16$^{o}$/mm, which is similar to the WT value of 93±13$^{o}$/mm (Figures 8E,8F).

Figures 5A-5C show the HOM map with smallest VFO, of 17%, with pixel distributions in Figure 1O. The projection from rostral colliculus is to most of the visual field (Figure 5B) and the small projection from caudal colliculus (Figure 5C) is to temporal field only. Figures 5D-5F show the map with largest VFO, of 59% with pixel distributions in Figure 1P. Apart from far-nasal visual field, there is a double representation on the colliculus.

In summary, highly ordered 2D maps from colliculus to visual field were reconstructed from noisy Fourier imaging data derived from both WT and EphA3 knockin mice. Sampling the colliculus at a spacing of 80 µm enables 2D maps to be constructed with around 90% of neighbouring points in the correct relative order and orientation.

In a WT map there is a single well-ordered map and HETA maps are identical to WT maps. In HETBs, HETCs and HOMs, the colliculus can be divided into two areas to produce two ordered maps. Figure 8A justifies this division, showing that more nodes are used in the two largest ordered partmaps than in the single map. The Visual Field Overlap (VFO) in the two partmaps varies both within and between groups. On average it is greater in the HOMs, less in the HETCs, and very small in the HETBs (Figure 8B). In HETCs and HOMs, the area of visual field that is represented in both areas is restricted to temporal field, nasal field tending to be absent from caudal colliculus (Figures 4,5). Azimuthal magnification is significantly greater in the rostral map than in the caudal map, being greatest in the HOM maps and least in HETB maps (Figures 8E, 8F). Figure 8 gives summary statistics for all 21 cases**.**

The large degree of variability within both HET and HOM maps suggests that they are derived from a continuum of single to double maps ranging from a single ordered map covering the colliculus to one with a projection of visual field from two distinct areas on the colliculus, more visual field represented rostrally than caudally.

Since these maps are from colliculus to visual field, they do not give information about where the two populations of EphA3+ and EphA3- ganglion cells project. It seems reasonable to conclude that in groups HETA and HETB, the projections from the populations of EphA3+ and EphA3- cells overlap completely or almost completely to give a single projection with little or no overlap in visual field, yielding effectively single wild type maps. The EphA3+/- map in Figure 1B might also be considered as single if the two separate projections onto caudal colliculus are not filtered out, as explained in the Legend to Figure1.
In double maps, one possibility is that EphA3+ cells project rostrally and EphA3- cells caudally as found in the homozygous Eph3 knockin maps by fibre tracing (Figure 1C; Brown et al., 2000). However, on this interpretation a substantial part of the representation of EphA3- cells on the caudal projection area would then be missing (Figures 4C, 4F, 5C, 5F). It seems unlikely that these missing representations of nasal field are to the central part of the colliculus which cannot be mapped by Fourier imaging because of interference between two projections because these projections would be from far-nasal and far-temporal field (Figure 1C), whereas in the HETC and HOM maps temporal field is always represented. Other possible interpretations are that in temporal retina (corresponding to nasal visual field) there are no EphA3- cells or that these cells are not functional.

*Insights from modelling studies*
To explore these issues requires study of double maps in which the projections from EphA3+ cells and from EphA3- cells to the colliculus can be related to the projections from colliculus to visual field supplied by Fourier-based intrinsic imaging. We looked at double maps obtained from the energy minimisation model (Triplett et al., 2011). To compare with the experimental maps, we made Lattice plots of the maps from colliculus to retina after applying our simulation of the Fourier imaging process to the model data**.** These maps were supplemented by Lattice plots from retina to colliculus, including separate maps of the EphA3+ and the EphA3- projections (see Methods).

Figure 6 shows a sequence of maps for different values of DR, the extra amount of EphA added to EphA3+ cells. With DR set at zero, in the collicular to retina projection, coloured black, rostral colliculus maps to temporal retina (visual field) and caudal colliculus to nasal retina (temporal field); there is a single map (Figure 6A). At a higher value of DR (Figure 6B), there is an area on the colliculus, coloured green and rejected by filtering, where the average retinal position varies considerably. This defines two distinct projection areas. The projection from rostral colliculus covers most of the retina whilst that from caudal colliculus remains to nasal retina, giving a measurable Visual Field Overlap (VFO). As DR is further increased,

the projection to nasal retina increases (Figures 6C, 6D), with larger VFO, until both rostral and caudal areas project to almost all of the retina (Figure 6E). Figures 8G, 8H shows statistics calculated over repeated runs on a smaller sized model to explore how average Map Quality and Visual Field Overlap depend on the value of DR.

These simulated maps from colliculus to retina can be related directly to the experimental maps and have several similar features. Simulated WT maps are single. A simulated EphA3 knockin map can be single, or a double map where the proportion of the retina (visual field) represented in both projection areas varies widely, depending on the value of the EphA+ augment, DR. In the double maps a larger extent of the retina is represented rostrally than caudally with much of temporal retina (nasal field) not represented in the caudal area. In the experimental maps there is significant variation, such as within the HOM category where either a small or a large extent of visual field is represented in rostral colliculus (Figures 5C, 5F). This difference could be attributed to the fact that, unlike in the simulations, signal strength varies considerably over the colliculus *(*Kalatsky and Stryker, 2003; Cang et al., 2008). The smaller amount of colliculus available for constructing the map after filtering may also explain why in the simulations, ordered maps of 400-500 nodes were constructed compared to 150-200 for the experimental maps.

Examination of the simulated projection from retina to colliculus now enables identification of the separate projections from the EphA3+ and the EphA3- cells. As described above, for DR=0, both EphA3+ and EphA3- cells from all parts of the retina project across the entire colliculus to give a single map. For a larger value of DR (blue maps, Figure 6B), the projection from EphA3+ cells is restricted to rostral colliculus and EphA3- cells project more widely so that rostral colliculus is innervated by both EphA3+ and EphA3- cells. At a larger value, the projection from EphA3- cells starts to become restricted to caudal colliculus with a strip of double innervation rostrally (Figure 6C), which then is smaller for larger DR. (Figure 6D). Ultimately EphA3+ cells project rostrally and EphA3- caudally to give a double representation of retina on the colliculus (Figure 6E). Figure 7 shows a set of 1D profiles for a series of maps with different values of DR to illustrate how these maps are formed, as described in the Legend. Rows 3 and 4 in Figure 7 illustrates the difference between the map of visual field seen from the colliculus and the map of colliculus seen from visual field.

There are two other relevant properties of the model (Gale and Willshaw, in preparation).

(1) The level of neural activity controls the tendency from neighbouring retinal cells to connect to neighbouring collicular cells. Lowering activity slows down the development of the projection in its earliest stages. This also reduces the number of EphA3+ and WT cells from the same retinal location projecting in register on rostral colliculus.

(2) In double maps the distribution and relative proportion of EphA3+ to EphA3- cells in the retina affect their patterns of innervation. For example, changing the percentage of cells that are EphA3+ changes the relative proportions of the colliculus innervated by the two populations.

We suggest that it is how the profile of EphA over the EphA3- cells compares with that over the EphA3+ cells which is crucial to determining the form of a EphA3+ knockin maps. If the profiles are almost identical, then Fourier-based imaging would show a single or near single map (HETA, Figure 2; HETB: Figure 3; Figures 6B,6C). More distinct profiles would result in a partially double map (HETC. Figure 4; HOM: Figure 5). According to the characterisation of

the EphA gradients by Reber et al, (2004) used in the model, Figures 6B and 7C would represent a EphA3+/- map and Figures 6D and 7F a EphA3+/+ map.

The modelling studies highlight the possibility that the absence of nasal visual field (temporal retina) in the projection from caudal colliculus in the experimental data is due to EphA3- cells and EphA3+ cells of temporal origin projecting in register to rostral colliculus. In EphA3+/- animals, evidence for such superposed projections in rostral colliculus has been found by axonal tracing (Figure 1B; Brown et al., 2004; Reber et al., 2004; Bevins et al., 2008: Owens et al. 2015). However, such a study needs to be linked to a specific map. For example, in Figure 5A-5C there should be a large, superposed projection; in Figures 5D-5F, there should little or none.
If there is no superposed projection in a map where nasal visual field is not represented in the caudal projection area, a possible explanation is that there is an inhomogeneity of retinal origin; for example, an inhomogeneous distribution of the EphA3 augment over the EphA3+ cells of the retina; or an inhomogeneous distribution of the Islet2 cells to which EphA3 is attached (Pak et al., 2004; Marcucci, 2019); or the contacts made by EphA3+ cells are more powerful than those made by EphA3- cells.

### *Comparison with previous analysis*

The original analysis of this dataset was made by Owens et al. (2015). They sampled the azimuthal map at three different tracks running rostrocaudally across the colliculus to draw conclusions about the nasotemporal to rostrocaudal ordering over the entire map. They characterised the maps according to whether the 1D projections along the three tracks are single, double or mixed, a mixture of single and double. They identified the WTs as single, the HOMs as double and they found HETs of all three types.
They then investigated possible sources of this diversity of projection in the HETS. They used a quantitative measure to classify the effects of (i) genetic variation by comparing maps from ipsilateral and contralateral colliculi and (ii) neural activity by looking at maps from animals with heterozygous knockin of EphA3 combined with homozygous or heterozygous knockouts of the β2 receptor, thought to disrupt retinal waves (Chandrasekaran et al., 2005; Stafford et al., 2009, Lyngholm et al., 2019)).

Combining these results, they concluded that the existence of single, double and mixed HET maps is evidence that the HET is an unstable state which can be switched between double and single configurations by small changes in, for example, the amount of additional EphA assigned to the EphA3+ cells or activity-dependent influences. They used a computational model to support the existence of this type of stochasticity.

The main differences between the two approaches are that Owens et al. (2015) examined data from the azimuthal scan only and represented the map by 1D profiles measured along three fixed tracks. From these three profiles a quantitative measure was used to classify the maps. We examined filtered data obtained from both azimuthal and elevational scans. This allowed three abnormal maps, which they had included in their analysis, to be rejected. We found that information extracted from fixed 1D profiles is sensitive to the positioning of the tracks (Figure 2) and so we preferred the more direct approach of reconstructing the entire 2D map.

We agree with Owens et al. (2015) in their interpretation of WTs and four of the HETs which we called HETAs as single projections. They regarded the HOMs as double maps and the

remaining nine HETs as mixed or doubles whereas we concluded that these maps are examples of a single population within which there is wide variation, such as in the extent of the Visual Field Overlap. According to the database, the case they presented as an example of a HET being a double map (their Figure 1N) was in fact a HOM (our Figures 1O, 5D-5F).

Due to the lack of matching azimuthal and elevational scans which is needed for our analysis, we were unable to replicate the analysis by Owens et al. (2015) in support of their hypotheses relating to possible genetic diversity and the role of neural activity. Their conclusions rely on a small number of cases and on the use of their own quantitative measure which they did not validate. However, we did repeat the simulations of a computational model which they used to support their stochastic hypothesis. This model, TK2006 (Tsigankov and Koulakov, 2006, 2010) is an earlier version of the one that we used in our analysis of the experimental data. We did not use this model in our analysis as it allows only one contact per cell, which disrupts the mapping, as described below.

We used the same set of parameters as Owens et al. (2015) and varied the magnitude of the EphA3 augment, DR, over a wide range. The maps in the 1st row of panels of Figures 8I-8M resemble their published maps**.** At low DR, there are single maps (Figure 8I) and at higher values completely double maps (Figure 8M). With a change of DR from 0.3 (Figure 8L) to 0.36 (Figure 8J), a single map changed into a blotchy map of the type that Owens et al. (2015) found, which transformed gradually into a double map over the range DR =0.36 to DR=0.7. (Figures 8J-8M). In contrast, Owens et al (2015) reported that a slight variation of DR around 0.36 would switch the map from single to double. When we plotted the projections from the EphA3+ and EphA3- retinal cells separately, shown in the panels in the rows 2 and 3, we found that the blotchy projections found for intermediate values of DR are due to neighbouring cells of the two types forming interleaving projections, each excluding the contacts from cells of the other type (Figures 8J-8L), similar to a pattern of zebra stripes This is a result of the strong competitive constraint of requiring one-to-one connectivity which masks the smooth variation from a single projection to a double projection as DR is increased.
In summary, as DR is increased from 0.3 to 0.7, the map evolves gradually from a single into a double map, by DR=0.7. We did not find any evidence in this model for small variations of DR producing rapid switching between the single and double states.

## Discussion

We present a detailed reanalysis of the ordered visuocollicular maps in EphA3 knockin mice generated by Fourier-based imaging. This method provides a mapping from colliculus to visual field and has its limitations for the analysis of double maps; a complete analysis would also require details of the mapping from visual field to colliculus. Within these limitations, we found that individual maps of both heterozygous and homozygous EphA3+ genotypes vary widely in terms of the extent of the visual field being duplicated on the two projection areas of the superior colliculus.

Aided by computer simulation studies, we suggest that what drives the formation of the single or double maps found in these mice is how the graded distribution of EphA over the EphA3+ ganglion cells in the retina compares with that over the EphA3- cells

From our results, it is difficult to argue for a stochastic model of map formation where in the EphA3+ knockin maps the heterozygous knockin represents an unstable transitory state between a single and a double projection (Owens et al., 2015).

Essential to our analysis has been the use of the Lattice method (Willshaw et al., 2014) which is ideal for the construction and analysis of ordered topographic maps to the scale required. In situations where large datasets are available, statistics derived from use of this method can be used in population studies generated either from experiment or from simulation (Figures 8G, 8H; Gale, PhD thesis).

Our maps of the experimental data are broadly consistent with an existing computational model (Triplett et al., 2011; Hjorth et al., 2015). We were not able to analyse the maps found in EphA3+ animals also subject to knockout of the Beta2 component of the acetylcholine receptor, which affects neural activity. However, we did find that lowering the strength of activity in the model reduces the extent to which EphA3+ and WT cells project in register on rostral colliculus. Given suitable data, this model can be challenged by constructing 2D maps for other EphA3+ mice to investigate the roles of genetic diversity and neural activity.

The chemoaffinity mechanism used in this model is of the graded matching type. This concept was introduced by Prestige and Willshaw (1975) in their analysis of retinotectal maps in non-mammalian vertebrates. It was presented as an alternative to direct matching where each retinal cell has maximum affinity to a small cluster of tectal cells; and vice versa **(**Sperry 1943,1963). Most of the proposed mechanisms of direct matching such as those incorporating double gradients (Rashid et al., 2005) and marker induction (von der Malsburg and Willshaw, 1977) incorporate a mechanism ensuring the retina projects over the entire target whatever their relative sizes. According to graded matching, when the cells in the retina are reduced substantially, only a small portion of the target will be innervated (Prestige and Willshaw, 1975). The maps found in mice lacking the gene Math5 (Lin et al., 2004) could be a way of distinguishing between direct and graded matching mechanisms. Math5 mice have 5–10% of the normal numbers of retinal ganglion cells which are spread evenly across the retina and innervate only a small portion of the colliculus (Triplett et al., 2011), although it is not known whether the map is ordered.

According to the model TK2011 that we analysed, the development of the retinocollicular map involves making contacts at random and removing contacts to decrease the energy of the system, representing the action of mechanisms of chemoaffinity, neural activity and competition. In common with all Markov Chain Monte Carlo methods (Brooks et al., 2011), it is not a true minimisation model which converges to a single configuration, but rather to a distribution of possible configurations (Gale, PhD thesis). Triplett et al (2011) discuss the need for the three mechanisms in the model, using biological data to justify some components and stability arguments for others.

One question is how far the process of making and discarding contacts in the model is intended to mimic development directly or is just a convenient way of finding a configuration of contacts with lowest energy. For the model to simulate the developmental process, its elements and operation must have direct counterparts in the biology. Other simpler graded matching models, such as ones involving the gradual addition of contacts rather than the withdrawal of contacts from an initial population, may be possible. In the original graded matching model due to Prestige and Willshaw (1975), contacts are made at random and

maintained for a period of time, which depends on their graded affinity. Reber et al. (2004) presented evidence for graded affinity but without presenting a formal model.

One key finding in our analysis of double maps is that part of the projection from nasal visual field to caudal colliculus was absent. Several possible explanations were given, which could be explored by combining anatomical studies on animals with known functional maps.
The clearest and possibly most feasible predictions from our analysis are to look at the properties of individual EphA3 knockin 2D maps to test out the relation between the form of the map and (i) the distribution of Islet2 cells in the retina and (ii) the location of collicular cells innervated by both EphA3+ and EphA3- cells.

## Methods

*Filtering the imaging data*

In Fourier based intrinsic imaging, the visual field is scanned in two orthogonal directions to determine separately the mapping of visual field positions along the nasotemporal axis onto the colliculus (azimuthal scan) and that of positions along the dorsoventral axis of visual field (elevational scan). Following Kalatsky and Stryker (2003), the location of the visual projection on the colliculus was defined as the region where excitation from visual field in the elevational map (dorsoventral scan) was highest, and an ellipse was drawn to enclose this region. Over this region the strength of the signal varied considerably and information from only the 10000 most active pixels was considered (Cang et al., 2008). By combining data from the azimuthal and elevational scans of the visual field, the visual field position providing maximal excitation at each pixel in the collicular image was then calculated (Willshaw et al., 2014).
A second stage of filtering was then necessary to remove unreliable information resulting from use of the Fourier imaging method. For each position on the colliculus, this yields a single position in the visual field. This is appropriate for a normal, single projection (Figure 1A), or for a complete double map (Figure 1D) where there is an ordered map to two separate areas of the colliculus. In these cases, a unique position in the visual field can be identified with each point on the colliculus. The visual field position identified with each small area of colliculus varies smoothly over the colliculus (except at the boundary between the two areas for Figure 1D). However, in cases where two small regions of visual field map to the same area of colliculus, as in the EphA3+/- and the EphA3+/+ knockins (Brown et al., 2000**;** Figures 1B, 1C, shaded green) or in two hypothetical mappings (Figures 1E, 1F), the visual field position recorded at any pixel will be very different from the two visual field positions and therefore wildly inaccurate. This average is liable to fluctuate from pixel to pixel (Willshaw et al., 2014). As a consequence, pixels for which the standard deviation of the mean visual field positions (red bar, Figures 1B, 1C,1E) was greater than three times than in WTs were removed from the analysis. Where the standard deviation was less than this amount (grey area, Figures 1B,1E, 1F) the pixels were retained.
The active pixels accepted after these two stages of filtering are called *eligible* and those discarded are called *rejected*. Visual field information derived from the set of eligible pixels was then used to construct 1D and 2D maps.

*Extension of 1D analysis*

To compare with the 1D analysis of Owens et al. (2015), we plotted out the variation of azimuthal phase, signalling the nasotemporal component of visual field, along three straight lines drawn on the colliculus. These represented the visual field at the three dorsoventral elevations of $25^o$, $0^o$ and $+25^o$. We found the projection onto the colliculus from all visual field positions at the given elevation and then made a straight line fit to these points. This line was then projected back onto the visual field and the corresponding visual field positions plotted.

*Construction of 2D maps – the Lattice Method*
We used the Lattice Method (Willshaw et al., 2014) which was developed to analyse a set of different set of Fourier-based intrinsic imaging data of the visuocollicular projection (Cang et al., 2008). Some of the eligible pixels were chosen at random to act as 'virtual electrodes', subject to there being a mean spacing of 6 pixel-widths (here equivalent to 80µm) between nearest neighbours. For each virtual electrode, we then calculated the mean position of all visual field points having corresponding collicular positions within a circle of radius 3 pixel-widths of the virtual electrode. This gave a one-to-one mapping between 150-200 virtual electrodes on the colliculus (*collicular node*s), spaced at approximately 80µm, and the same number of averaged visual field positions (*visual nodes*). The spacing between collicular nodes was chosen to be the smallest that gives highly ordered 2D maps in WTs, as found in a previous analysis (Willshaw, unpublished observations).

Neighbouring collicular nodes were then interconnected to form a lattice. The nodes in the visual field which are associated with interconnected collicular nodes were then interconnected. If the resulting structure constructed in the visual field is also a lattice, with no edges crossing, then local order is preserved because each pair of neighbouring visual nodes would then connect to a pair of neighbouring collicular nodes. Generally, this is not the case and by removing pairs of matching visual and collicular nodes, one by one, we found the largest ordered submap in which the remaining visual nodes form a lattice. Map Quality, the proportion of nodes remaining in the largest ordered submap, is a measure of the degree of local order. More details about the Lattice Method are given in Willshaw et al. (2014), including our method for removing nodes.

In cases where two projection areas on the colliculus could be defined, two separate partmaps were also constructed from the two lattices made from the nodes in each of these areas. This removed the interference caused by a portion of the visual field being represented in both areas.

Global properties of the map were measured in the largest ordered submap, by comparing the properties of the lattice and the corresponding visual field lattice so formed. They are assessed along two orthogonal axes after rotating the projection in visual space by $20^{o}$ to allow for the fact that in WT maps the nasotemporal axis projects at this angle onto the rostrocaudal axis (Dräger and Hubel 1976; Willshaw et al., 2014).
Rostrocaudal polarity (RCP) is the proportion of edges in the visual lattice which project onto the colliculus in the same relative rostrocaudal order as they would in a perfectly ordered map. A score of 100% represents perfect ordering along the rostrocaudal axis, 50% indicates random order and perfect but reversed order is 0%. Mediolateral polarity (MLP) is calculated similarly.
Magnification ratio is a measure of the relative extent of the projection along a specified axis. The Azimuthal Magnification (AM) is the length of each edge in the visual lattice measured along the rotated nasotemporal axis of visual field compared to the length of the corresponding edge in the collicular lattice measured along the rostrocaudal axis; similarly for the Elevational Magnification (EM).

In cases when two partmaps were constructed by partitioning the colliculus, the extent of visual field which are represented in both regions of the colliculus, called the Visual Field Overlap (VFO), was measured. In a completely double map, the VFO is the entire extent of visual field (Figure 1D). In the homozygous knockin shown in Figure 1C there is a partial double map with the area of colliculus holding a projection from two distinct regions of visual field situated far nasally and far temporally (green area), which is not measurable accurately

with Fourier imaging, as described above. Here the VFO is smaller than in Figure 1D. In the heterozygous knockin (Figure 1B) the VFO is zero.

*Computer simulations.*
A computational model **(**Triplett et al., 2011; Hjorth et al., 2015**)** for the development of a retinocollicular map, here called TK2011, was used to help to understand the data.
In this model, retina and colliculus are each laid out as a 2D array of cells. The mapping is built up by iteratively creating and deleting contacts stochastically to reduce a quantity called the energy, calculated over all contacts, which reflects the influences of chemoaffinity, neural activity and competition. Each cell may have more than one contact.
Each newly created contact is chosen by sampling uniformly from all possible pairs of cells and similarly each possible deletion is chosen from the existing set of contacts. The chemoaffinity energy is calculated from the gradients of EphA and EphB labelling the two axes of the retina and the matching gradients of ephrinA and ephrin B in the colliculus. For a retinal cell with an amount $R_A$ of EphA and a collicular cell with an amount $C_A$ of ephrinA, the contribution to the energy for the contact between them is $R_A*C_A$. This favours contacts between cells with high EphA and those with low ephrinA, and vice versa, which replicates the directions of the EphA and ephrinA gradients found experimentally (Cheng et al., 1995; Flanagan and Vanderhaeghen, 1998). In the EphB/ephrinB system, high EphB maps to high ephrinB (McLaughlin et al., 2003a) and so the contribution to the energy is $-R_B*C_B$. The contribution from electrical activity favours the development of contacts from neighbours to neighbours and the competitive mechanism prevents cells from having too many or too few contacts.

We carried out an extensive set of simulations of the development of the retinocollicular map using the code for TK2011 developed by Hjorth et al. (2015). To match to the number of data points selected for analysis of the experimental data (Cang et al., 2008), 10000 retinal cells were distributed randomly within a circular retina subject to a minimal distance between neighbours. 10000 collicular cells were distributed in the same way, over a hemiellipse representing the shape of the colliculus. The shapes of the EphA profiles were taken from Reber et al. (2004), with values scaled so that in the wildtype they were between 0 and 1. We used the parameter values from Triplett et al. (2011) except that the magnitude of the activity term in the energy was scaled to ensure that in the WT virtual injections into 1% of the retinal area innervated 1% of the colliculus (McLaughlin et al., 2003b) and we ran each simulation for a larger number of iterations, $5X10^8$ against $1.4X10^7$. The knockin of EphA3 was modelled by adding an extra amount of EphA, DR, to approximately 50% of the population of retinal cells. Choosing an equal number of cells of the two types avoids giving a competitive advantage to EphA3+ or EphA3- cells due to different numbers of cells. Parameter values are summarised in the legend to Figure 8. For EphA3+/+ knockins the value of DR was assumed to be twice that for EphA3+/- knockins (Brown et al., 2000). To assess the variation due to the random positioning of cells and the random assignment of retinal cells as EphA3+, a number of runs on a reduced 2000X2000 system was carried out for each value of DR. The maps were constructed using the Lattice method (Willshaw et al., 2014).

To model the experimental results precisely we then made a functional map by taking the modelled anatomical data obtained from the initial simulations and then replicating the Fourier imaging method. We simulated the repeated scanning of the retina in two orthogonal directions using a bar with a width of 2% of the linear extent of the retina **(**Kalatsky and Stryker, 2003). Retinal and collicular firing were calculated using a Poisson model, with

retinal firing rate proportional to the location of the bar and collicular firing rate calculated from the transmission of retinal spikes through the contacts formed and the transmission of collicular spikes through local excitation and inhibition (Phongphanphanee, 2012). In order to extract the mapping of collicular position onto retinal position, we then carried out Fourier analysis on the time course of the activity pattern at the repetition frequency. We constructed the map from colliculus to retina, which corresponds to the experimental maps found by Fourier intrinsic imaging. We also constructed simulated maps to the colliculus from the whole retina and from the separate subpopulations of EphA3+ and EphA3- retinal ganglion cells. In the latter two cases, the scan was restricted to the subpopulation in question.

We also simulated an earlier version of this model (Tsigankov and Koulakov, 2006, 2010), here called TK2006, to compare with the modelling results from Owens et al. (2015), who used this model (Tsigankov and Koulakov, 2006, 2010). The crucial difference between the two models is that in TK2006, each collicular cell makes a single contact. This removes the need for a competition term in the energy function but introduces discontinuities in the mapping.

*Access to resources.*
For access to the experimental data, please refer to Owens et al. (2015), where the data was first reported. The simulation code for TK2011 developed by Hjorth et al. (2015), is available at https://github.com/Hjorthmedh/RetinalMap. The entire code used for the analysis of the experimental and the simulation data is not yet available and the current version is at https://github.com/Nick-Gale/Lattice_Method_Analysis_EphA3_Mutants.

**Acknowledgements.** This research was funded in whole, or in part, by the Wellcome Trust (Programme Grant number W083205A (DW) and PhD grant (number 215153/Z/18/Z (NG)). Our thanks for support to ANC (University of Edinburgh) and DAMTP (Cambridge) and to Stephen Eglen, David Price, Geoff Goodhill and Peter Dayan for their comments. Special thanks to Jason Triplett for comments and for sharing the experimental data with us. For the purpose of open access, the authors have applied a CC BY public copyright licence to any Author Accepted Manuscript version arising from this submission.

**Author Contributions**. DJW secured funding, conceived the project, carried out the experimental data analysis and wrote the paper. NMG secured funding, collaborated in project design, carried out the computational modelling and wrote the paper.

**Declaration of Interests.** The authors declare no competing interests.

## References


Bevins, N., Lemke, G., & Reber, M. (2011). Genetic dissection of EphA receptor signaling dynamics during retinotopic mapping. *Journal of Neuroscience*, *31*(28), 10302-10310.

Brooks, S., Gelman, A., Jones, G., & Meng, X. L. (Eds.). (2011). *Handbook of Markov Chain Monte Carlo*. CRC press.

Brown, A., Yates, P. A., Burrola, P., Ortuño, D., Vaidya, A., Jessell, T. M., & Lemke, G. (2000). Topographic mapping from the retina to the midbrain is controlled by relative but not absolute levels of EphA receptor signaling. *Cell*, *102*(1), 77-88.

Brown, N. L., Patel, S., Brzezinski, J., & Glaser, T. (2001). Math5 is required for retinal ganglion cell and optic nerve formation.

Cang, J., & Feldheim, D. A. (2013). Developmental mechanisms of topographic map formation and alignment. *Annual review of neuroscience*, *36*, 51-77.

Cang, J., Wang, L., Stryker, M. P., & Feldheim, D. A. (2008). Roles of ephrin-as and structured activity in the development of functional maps in the superior colliculus. *Journal of Neuroscience*, *28*(43), 11015-11023.

Chandrasekaran, A. R., Plas, D. T., Gonzalez, E., & Crair, M. C. (2005). Evidence for an instructive role of retinal activity in retinotopic map refinement in the superior colliculus of the mouse. *Journal of Neuroscience*, *25*(29), 6929-6938.

Cheng, H. J., Nakamoto, M., Bergemann, A. D., & Flanagan, J. G. (1995). Complementary gradients in expression and binding of ELF-1 and Mek4 in development of the topographic retinotectal projection map. *Cell*, *82*(3), 371-381.

Drager, U. C., & Hubel, D. H. (1976). Topography of visual and somatosensory projections to mouse superior colliculus. *Journal of Neurophysiology*, *39*(1), 91-101.

Finlay, B. L., Schneps, S. E., Wilson, K. G., & Schneider, G. E. (1978). Topography of visual and somatosensory projections to the superior colliculus of the golden hamster. *Brain research*, *142*(2), 223-235.

Flanagan, J. G., & Vanderhaeghen, P. (1998). The ephrins and Eph receptors in neural development. *Annual review of neuroscience*, *21*(1), 309-345.

Gale, N. M. (2022). *PhD thesis*, University of Cambridge.

Hjorth, J. J., Sterratt, D. C., Cutts, C. S., Willshaw, D. J., & Eglen, S. J. (2015). Quantitative assessment of computational models for retinotopic map formation. *Developmental neurobiology*, *75*(6), 641-666.

Kalatsky, V. A., & Stryker, M. P. (2003). New paradigm for optical imaging: temporally encoded maps of intrinsic signal. *Neuron*, *38*(4), 529-545.

King, A. J., Schnupp, J. W., Carlile, S., Smith, A. L., & Thompson, I. D. (1996). The development of topographically-aligned maps of visual and auditory space in the superior colliculus. In *Progress in brain research* (Vol. 112, pp. 335-350). Elsevier.

Lin, B., Wang, S. W., & Masland, R. H. (2004). Retinal ganglion cell type, size, and spacing can be specified independent of homotypic dendritic contacts. *Neuron*, *43*(4), 475-485.

Lyngholm, D., Sterratt, D. C., Hjorth, J. J., Willshaw, D. J., Eglen, S. J., & Thompson, I. D. (2019). Measuring and Modelling the Emergence of Order in the Mouse Retinocollicular Projection. *bioRxiv*, 713628.

McLaughlin, T., Hindges, R., & O'Leary, D. D. (2003a). Regulation of axial patterning of the retina and its topographic mapping in the brain. *Current opinion in neurobiology*, *13*(1), 57-69.

McLaughlin, T., Torborg, C. L., Feller, M. B., & O'Leary, D. D. (2003b). Retinotopic map refinement requires spontaneous retinal waves during a brief critical period of development. *Neuron*, *40*(6), 1147-1160.

Marcucci, F., Soares, C. A., & Mason, C. (2019). Distinct timing of neurogenesis of ipsilateral and contralateral retinal ganglion cells. *Journal of Comparative Neurology*, *527*(1), 212-224.

Owens, M. T., Feldheim, D. A., Stryker, M. P., & Triplett, J. W. (2015). Stochastic interaction between neural activity and molecular cues in the formation of topographic maps. *Neuron*, *87*(6), 1261-1273.

Pak, W., Hindges, R., Lim, Y. S., Pfaff, S. L., & O'Leary, D. D. (2004). Magnitude of binocular vision controlled by islet-2 repression of a genetic program that specifies laterality of retinal axon pathfinding. *Cell*, *119*(4), 567-578.

Pfeiffenberger, C., Yamada, J., & Feldheim, D. A. (2006). Ephrin-As and patterned retinal activity act together in the development of topographic maps in the primary visual system. *Journal of Neuroscience*, *26*(50), 12873-12884.

Phongphanphanee, P., Marino, R. A., Kaneda, K., Yanagawa, Y., Munoz, D. P., & Isa, T. (2014). Distinct local circuit properties of the superficial and intermediate layers of the rodent superior colliculus. *European Journal of Neuroscience*, *40*(2), 2329-2343.

Prestige, M. C., & Willshaw, D. J. (1975). On a role for competition in the formation of patterned neural connexions. *Proceedings of the Royal Society of London. Series B. Biological Sciences*, *190*(1098), 77-98.

Rashid, T., Upton, A. L., Blentic, A., Ciossek, T., Knöll, B., Thompson, I. D., & Drescher, U. (2005). Opposing gradients of ephrin-As and EphA7 in the superior colliculus are essential for topographic mapping in the mammalian visual system. *Neuron*, *47*(1), 57-69.

Reber, M., Burrola, P., & Lemke, G. (2004). A relative signalling model for the formation of a topographic neural map. *Nature*, *431*(7010), 847-853.

Sperry, R. W. (1943). Visuomotor coordination in the newt (Triturus viridescens) after regeneration of the optic nerve. *Journal of comparative neurology*, *79*(1), 33-55.

Sperry, R. W. (1963). Chemoaffinity in the orderly growth of nerve fiber patterns and connections. *Proceedings of the National Academy of Sciences of the United States of America*, *50*(4), 703.

Stafford, B. K., Sher, A., Litke, A. M., & Feldheim, D. A. (2009). Spatial-temporal patterns of retinal waves underlying activity-dependent refinement of retinofugal projections. *Neuron*, *64*(2), 200-212.

Triplett, J. W., Pfeiffenberger, C., Yamada, J., Stafford, B. K., Sweeney, N. T., Litke, A. M., & Feldheim, D. A. (2011). Competition is a driving force in topographic mapping. *Proceedings of the National Academy of Sciences*, *108*(47), 19060-19065.

Tsigankov, D. N., & Koulakov, A. A. (2006). A unifying model for activity-dependent and activity-independent mechanisms predicts complete structure of topographic maps in ephrin-A deficient mice. *Journal of computational neuroscience*, *21*(1), 101-114.

Tsigankov, D., & Koulakov, A. A. (2010). Sperry versus Hebb: Topographic mapping in Isl2/EphA3 mutant mice. *BMC neuroscience*, *11*(1), 1-15.

von der Malsburg, C., & Willshaw, D. J. (1977). How to label nerve cells so that they can interconnect in an ordered fashion. *Proceedings of the National Academy of Sciences*, *74*(11), 5176-5178.

Willshaw, D. (2006). Analysis of mouse EphA knockins and knockouts suggests that retinal axons programme target cells to form ordered retinotopic maps. *Development*, *133*(14), 2705-2717.

Willshaw, D. J., & von der Malsburg, C. (1979). A marker induction mechanism for the establishment of ordered neural mappings: its application to the retinotectal problem. *Philosophical Transactions of the Royal Society of London. B, Biological Sciences*, *287*(1021), 203-243.

Willshaw, D. J., Sterratt, D. C., & Teriakidis, A. (2014). Analysis of local and global topographic order in mouse retinocollicular maps. *Journal of Neuroscience*, *34*(5), 1791-1805.

## Figure Legends

**Figure 1**. One-dimensional profiles.

**A-F.** Projections of the nasotemporal axis of retina, depicted as visual field, onto the rostrocaudal axis of the superior colliculus. **A**. Wildtype. **B**. Heterogeneous EphA3 knockin (EphA3+/-). **C**. Homogeneous EphA3 knockin (EphA3+/+). All redrawn from Brown et al. (2000). **D-F**. three different types of hypothetical double map.

Purple: projection from EphA3+ cells; orange: projection from EphA3+ cells. The black vertical line shows the extent of visual field where there is a projection from both EphA3+ cells rostrally and EphA3- cells caudally, measured as the Visual Field Overlap (VFO). In **B**, **C, E** and **F**, the shaded region shows the part of the map where EphA3- cells and EphA3+ cells project to the same location. The filtering method used in the experimental data analysis removes the part of this double projection (shaded green) where the two visual field positions are further than a critical distance (red bar) apart. Where the two positions are within this distance they are reported as a single map (grey area; dotted brown line).

R: rostral; C: caudal; N: nasal; T: temporal.

**G-R.** Examples from the database of the distribution of the variation of the azimuthal (nasotemporal) component of phase recorded along three straight lines drawn on the colliculus representing 1D sections at three standard elevations of -25$^{o}$ (orange), 0$^{o}$ (cyan) and +25$^{o}$ (brown) for WT, heterozygous (EphA3+/-) and homozygous (EphA3+/+) knockins. **G, H**. WT. **I-N,Q**. EphA3+/-. **O, P, R**. EphA3+/+.

Rows 1,2: the distributions of eligible (grey) and rejected (green) visual field positions and pixels. Each coloured line on the colliculus (row 2) is the straight line fit to the positions of all eligible pixels where the corresponding visual field positions are at the given elevation. The coloured points plotted on the visual field representation (row 1) is the projection back into the visual field of all the pixels on the straight line. Black dotted lines show the tracks used by Owens et al. (2015) in sampling the projection.

Row 3-5: Plots of the azimuthal component of phase against collicular position along the appropriate 1D section. The orientation of the 1D sections vary but are all at approximately 20$^{o}$ to the rostro-caudal axis. All three plots for the same dataset are drawn with the same horizontal scale, which varies from dataset to dataset.

Units: visual field: degrees; colliculus: mm.

**Figure 2**

2D maps from colliculus (bottom) to visual field (top) for WT and HETA datasets. Neighbouring nodes on the colliculus and the corresponding nodes in the visual field map are connected by straight lines. Lines in the visual field which cross and the corresponding lines on the colliculus are coloured red. To relate the 2D maps to the patterns of 1D profiles in Figure 1, three lines representing the projection at -25$^o$ (orange), 0$^o$ (cyan) and +25$^o$ (brown) are shown.

**A**. The complete projection with 162 nodes for the WT shown in Figure 1G**.**

**B**. The largest ordered submap, constructed by removing 4% of the nodes from the complete projection to eliminate all crossing lines. RC, ML polarities: all 90%.

**C**. The largest ordered submap for the HETA shown in Figure 1I, with 215 nodes in the whole map. Map Quality: 86%. RC, ML polarities: all 90%. Azimuthal and Elevational Magnifications: 77$^o$/mm, 60$^o$/mm.

**D**. The complete projection, with 165 nodes, for the WT shown in Figure 1H.

**E**, **F**. The two largest ordered sub-partmaps constructed on the two sets of nodes by partitioning the collicular nodes with a line drawn through the narrow strip of rejected pixels in rostral colliculus. **E**. Sub-partmap on rostral colliculus. **F**. Sub-partmap on the rest of the colliculus. RC, ML polarities are 94%. AM, EM: 115$^o$/mm, 58$^o$/mm.

D: dorsal, V: ventral; N: nasal; T: temporal. M: medial; L; lateral; R: rostral; C: caudal. Scale bars: 20$^o$ (visual field); 200µm (colliculus).

**Figure 3**

2D maps for two HETB datasets.

**A**. The largest ordered submap formed from the 148 nodes in the complete map for the HETB shown in Figure 1K. Map Quality: 84%

**B**, **C**. Sub-partmaps formed after partitioning the colliculus through the green areas of discarded pixels into rostral (**B**) and caudal (**C**) areas. 3% more nodes were recruited in the two sub-partmaps than in the largest ordered submap, giving a Map Quality of 87%. Visual Field Overlap (VFO), the area of visual field contained in both rostral and caudal projections: 3%. RC, ML polarities and AM, EM: 94%,89%, 118$^{o}$/mm, 89$^{o}$/mm (**B**); 68%, 83%, 84$^{o}$/mm, 75$^{o}$/mm (**C**).

**C.** The largest ordered submap formed from the 186 nodes in the complete map for the HETB shown in Figure 1L. Map Quality: 91%

**D**, **E**. Rostral and caudal sub-partmaps, with 3% more nodes than in **A**. VFO: 7%. RC, ML polarities and AM, EM: 96%, 92% 101$^{o}$/mm, 92$^{o}$/mm (**D**); 68%, 92%, 86$^{o}$/mm, 62$^{o}$/mm (**E**). Conventions as in Figure 2.

**Figure 4**

2D maps for the two HETC datasets.

**A**. The largest ordered submap formed from the 180 nodes in the complete map, for the HETC shown in Figure IM. Map Quality: 75%

**B**, **C**. Sub-partmaps, with Map Quality of 85% 11% more than in **A**. VFO: 29%. RC, ML polarities and AM, EM: 91%, 85%, 168$^{o}$/mm, 84$^{o}$/mm (**B**); 90%,88%, 88$^{o}$/mm, 73$^{o}$/mm (**C**). The value of AM for **B** is almost twice that for **C**, primarily due to the high magnification in temporal field.

**D**. The largest ordered submap formed from the 207 nodes in the complete map, for the HETC shown in Figure 1N. Map Quality: 91%

**E,F**. Sub-partmaps, with Map Quality 98%, 7% more than in **A**. VFO: 29%. All polarities between 90% and 93%. AM, EM: 160$^{o}$/mm, 82$^{o}$/mm (**E);** 86$^{o}$/mm, 76$^{o}$/mm (**F).** Conventions as in Figure 2.

**Figure 5**

2D maps for the two HOM datasets.

**A**. The largest ordered submap formed from the 148 nodes in the complete map for the HOM shown in Figure 1O. Map Quality: 83%

**B**, **C**. Sub-partmaps, with Map Quality of 93%, 10% more than in **A**. VFO: 17%. All polarities between 86% and 91%. AM, EM: 212$^{o}$/mm, 85$^{o}$/mm (**B);** 79$^{o}$/mm, 85$^{o}$/mm (**C).**

**D**. The largest ordered submap formed from the 148 nodes in the complete map, for the HOM shown in Figure 1P. Map Quality: 74%

**E**, **F**. Sub-partmaps, with Map Quality of 98%. 24% more than in **D**. VFO: 63%. All polarities between 91% and 93%. AM, EM: 174$^{o}$/mm, 117$^{o}$/mm (**E);** 140$^{o}$/mm, 85$^{o}$/mm (**F).**

Conventions as in Figure 2.

**Figure 6**

Single runs of the TK2011 model (Triplett et al., 2011). Connections developed between 10000 retinal cells and 10000 collicular cells, using the code due to Hjorth et al. (2015). Maps were computed for different values of DR, the amount of EphA added to the EphA3+ cells, and constructed using the Lattice Method (Willshaw et al., 2014). Largest ordered sub-partmaps are shown. Retina is plotted as visual field to aid comparison with the experimental plots. For the mapping from colliculus to retina, coloured black, the collicular lattice was divided into two by a line through the centre of the green (rejected) pixels. The lefthand plot is the map from the rostral part; the righthand plot that from the caudal part. For the mapping from retina to colliculus, coloured blue, the lefthand plot is the projection from EphA3+ cells and the righthand plot for the EphA3- cells .

**A.** DR=0. Colliculus to retina map only. The collicular lattice was divided into equal-sized rostral and caudal halves.

**B-E.** Projections in both directions are shown, for DR = 0.22, 0.34, 0.56. The shaded region in the retina is represented in both rostral and caudal collicular areas.

**F**. DR=1.12. Colliculus to retina map only.

Each retinal cell was chosen to be EphA3+ with probability 0.5.

Parameter values. $\alpha$=90, $\beta$=135, a=0.03,b=0.11 (Triplett el., 2012; Hjorth et al., 2015); $\gamma$=0.00625, $5X10^8$ iterations, (Gale, 2022).

The EphA gradient is derived from Reber et al. (2004). Values of DR quoted are expressed as a fraction of the span of EphA in a WT cell. On this scale, the values of DR for a EphA3+/- and a EphA3+/+ (Reber et al., 2004) are 0.26 and 0.52 respectively.

| Figure | A | B | C | D | E |
|---|---|---|---|---|---|
| DR | 0.0 | 0.226 | 0.339 | 0.55 | 1.12 |
| Number of nodes | 485 | 436 | 415 | 426 | 407 |
| VFO | 1 | 47 | 58 | 74 | 76 |
| MAP QUALITY (whole map) | 97 | 80 | 74 | 54 | 73 |
| MAP QUALITY (partmaps) | 98 | 95 | 96 | 95 | 95 |

**Figure 7**

A sequence of six simulated mappings of nasotemporal retina onto rostrocaudal colliculus, where the value of DR was increased in equal steps. Retina plotted as visual field.
Each subfigure has 5 separate plots.
Row 1: Distribution of EphA3- (purple) and EphA3+ (orange) cells over the retina. Blue marks the site of a simulated injection of 1% of the retinal cells.
Row 2: The distribution of EphA along the nasotemporal axis of the retina for both EphA3- cells (purple) and EphA3+ (orange) cells and of ephrinA (magenta) across the rostrocaudal axis of the colliculus.
Row 3: Nasotemporal component of the positions of all retinal cells with contacts from the colliculus cells lying along the rostrocaudal axis of the colliculus at mediolateral position 0.5, marked in row 5.
Row 4: Rostrocaudal component of the positions of all collicular cells with contacts from the retinal cells lying along the nasotemporal axis of the retina at dorsoventral position 0.5, shown in row 5. The projections from the EphA3 cells (purple) and the EphA3+ cells (orange) can be distinguished.
Row 5. Distribution of the average positions of the projections from each retinal cell, with the projections from the injected cells in blue.

Initially a large number of contacts is made at random and then contacts are withdrawn selectively, those that lower the overall energy being maintained. The difference in energy between the contacts made by two retinal cells on the same collicular cell is the product of the amounts of EphA and ephrinA present. Therefore, the cell with higher energy tends to be withdrawn as this decreases the energy by a larger amount.

**7A.** DR=0.0. EphA3- and EphA3+ cells at the same retinal location have the same amount of EphA and so there is a single map (Figure 7A).
**7B.** DR=0.113. Some WT cells from nasal retina (temporal visual field) have values of EphA lower than those in the EphA3+ population at the same collicular position (row 2, grey bar) and so survive at the expense of the contacts from the EphA3+ cells there. The contacts made more centrally by these same EphA3+ cells now compete against the EphA3- cells there, which have higher energy. These EphA3+ cells tend to survive, and the overall effect is that the EphA3+ projection from nasal retina is more central.
**7C,** DR=0.226 (Figure 6B) **, 7D,** DR=0.339 (Figure 6C). There is a growing population of EphA3- cells with unique values of EphA, increasing the extent of the single EphA3- projection caudally and leading to contacts from more and more EphA3+ cells being removed from this region of the colliculus. There is still a double projection far rostrally, where the activity mechanism favouring neighbour-neighbour connections dominates over the weaker chemoaffinity mechanism.
**7E**, DR=0.452; **7F**, DR=0.565 (Figure 6D)**.** A very strong EphA3+ projection centrally, results in increased pressure to maintain neighbourhood relations there by lowering the energy of the EphA3- contacts which out-compete the EphA3+ contacts and effectively break the EphA3- projection there. As DR is increased, the effect of chemoaffinity rostrally becomes stronger, diminishing the superposed projection.
For sufficiently large DR, all the WT cells have values of EphA lower than the EphA3+ cells and a double projection results. EphA3+ cells project rostrally and WT cells caudally.

**Figure 8**

Summary and controls for both experimental and modelling data.

**A-F.** Summary data for the 21 experimental maps analysed.

**A**. Map Quality of the two partmaps plotted against Map Quality for the whole map. For the single maps identified in the WT and HETA categories, the same Map Quality is plotted on both axes. **B**. For the HETs and the HOMs where two projection areas could be identified, the relation between the proportion of visual field represented in the rostral area compared to that in thecaudal area. The magnitude of the Visual Field overlap (VFO) is the length of the straight line to the off-diagonal.

**C**, **D.** Rostrocaudal (RC) polarity plotted against mediolateral (ML) polarity in double maps for the rostral map (**C**) and the caudal map (**D)**.

**E**, **F.** Azimuthal magnification (AM) plotted against elevational magnification (EM) in double maps for the rostral map (**E**) and the caudal map (**F)**. In **C-F**, data from the single maps is included.

**G, H.** Summary data for multiple simulations carried out on a model of reduced size for different amounts of the EphA3 knockin, DR. **G.** Visual Field Overlap (VFO). **H**. Map quality. 2000 retinal cells and 2000 collicular cells, $2X10^7$ iterations per run. 100 runs for each value of DR. Mean shown by the horizontal line within the box, which encloses one quarter of the data points. Standard deviation shown by the vertical line.

**I-M.** Maps generated by simulations of the TK2006 model (Tsigankov and Koulakov, 2006) for five different values of the EphA3 augment, DR, to be compared with those in Figure 7 of Owens at al. (2015), using the same code (Reber, pers. comm.).

The retinal cells are labelled according to their position along the nasotemporal axis by five stripes of different colours (Owens et al., 2015). For each value of DR, there are three maps showing the colour-coded nasotemporal origins of the retinal cells (plotted as visual field) projecting to each part of the colliculus. Row 1: projection from all cells; row 2: projection from EphA3+ cells; row 3: projection from EphA3- cells.

**I**: DR=0.3 (0.35); **J**: DR=0.36 (0.42); **K**: DR=0.4 (0.46); **L**: DR=0.5 (0.58); **M**: DR=0.7 (0.81). The values in parentheses are according to the convention used for TK2011, to aid comparison with the simulations shown in Figures 6-7.

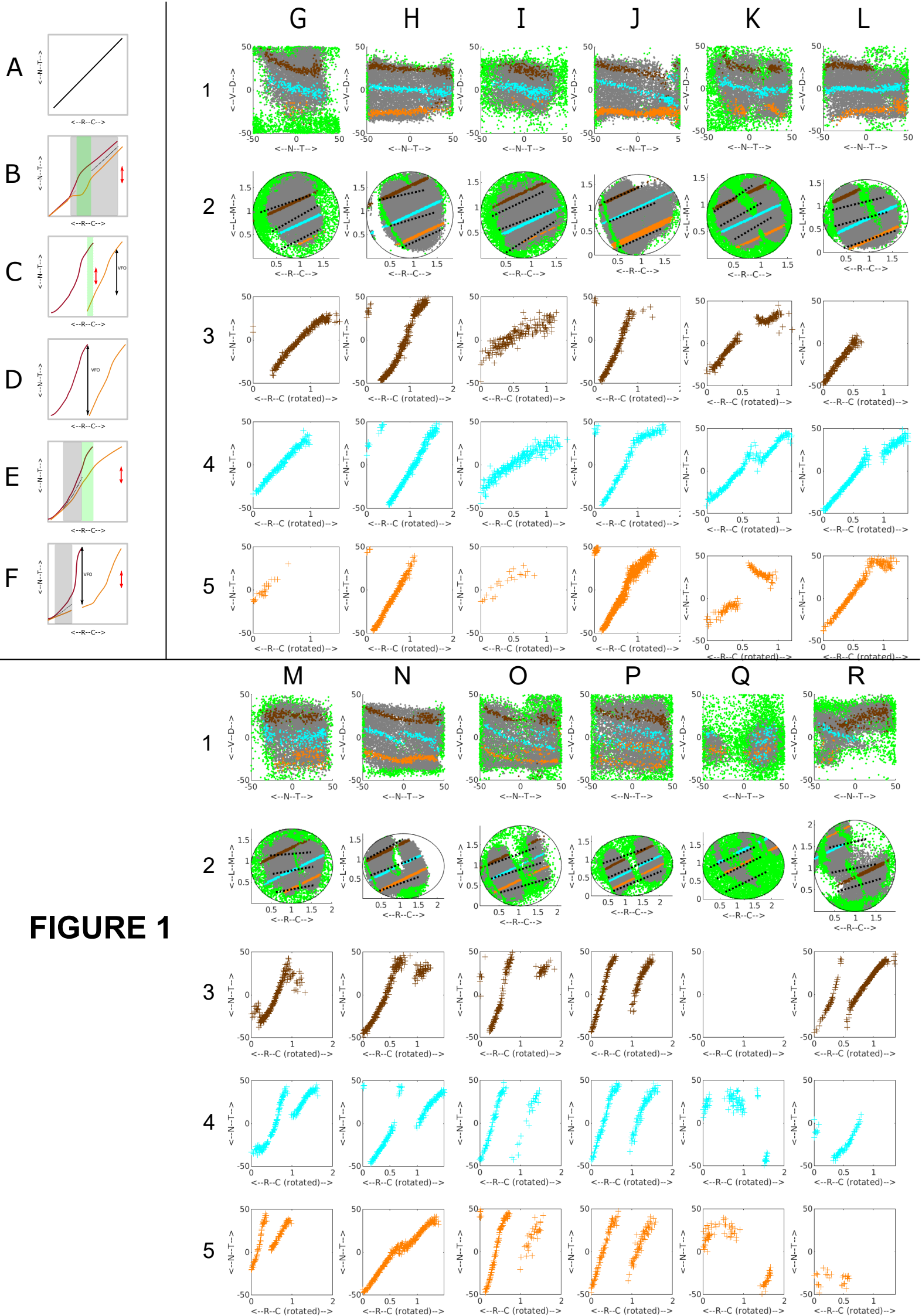


**FIGURE 1**

# FIGURE 2

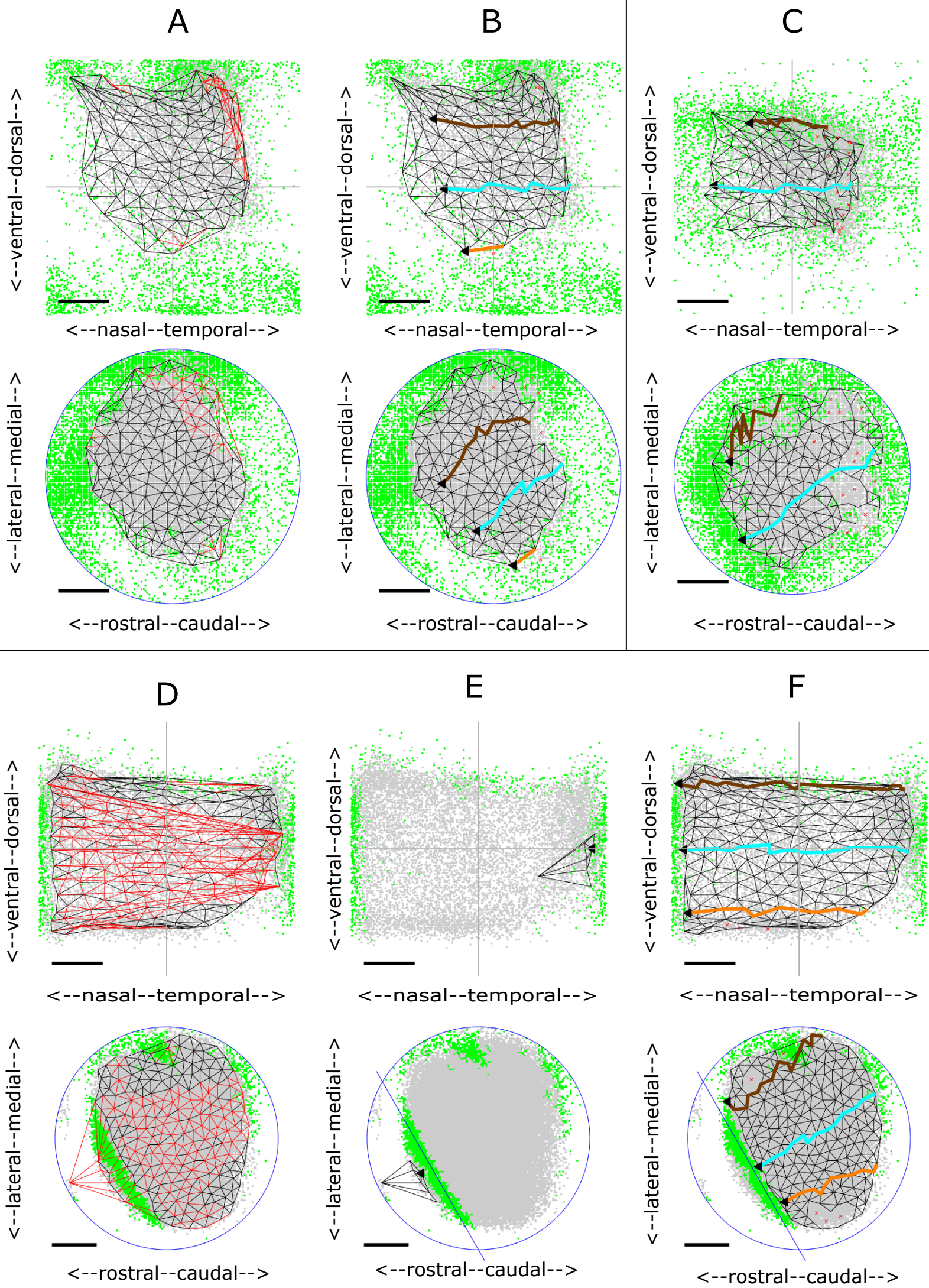
A
B
C
D
E
F
<--ventral--dorsal-->
<--nasal--temporal-->
<--lateral--medial-->
<--rostral--caudal-->

# FIGURE 3

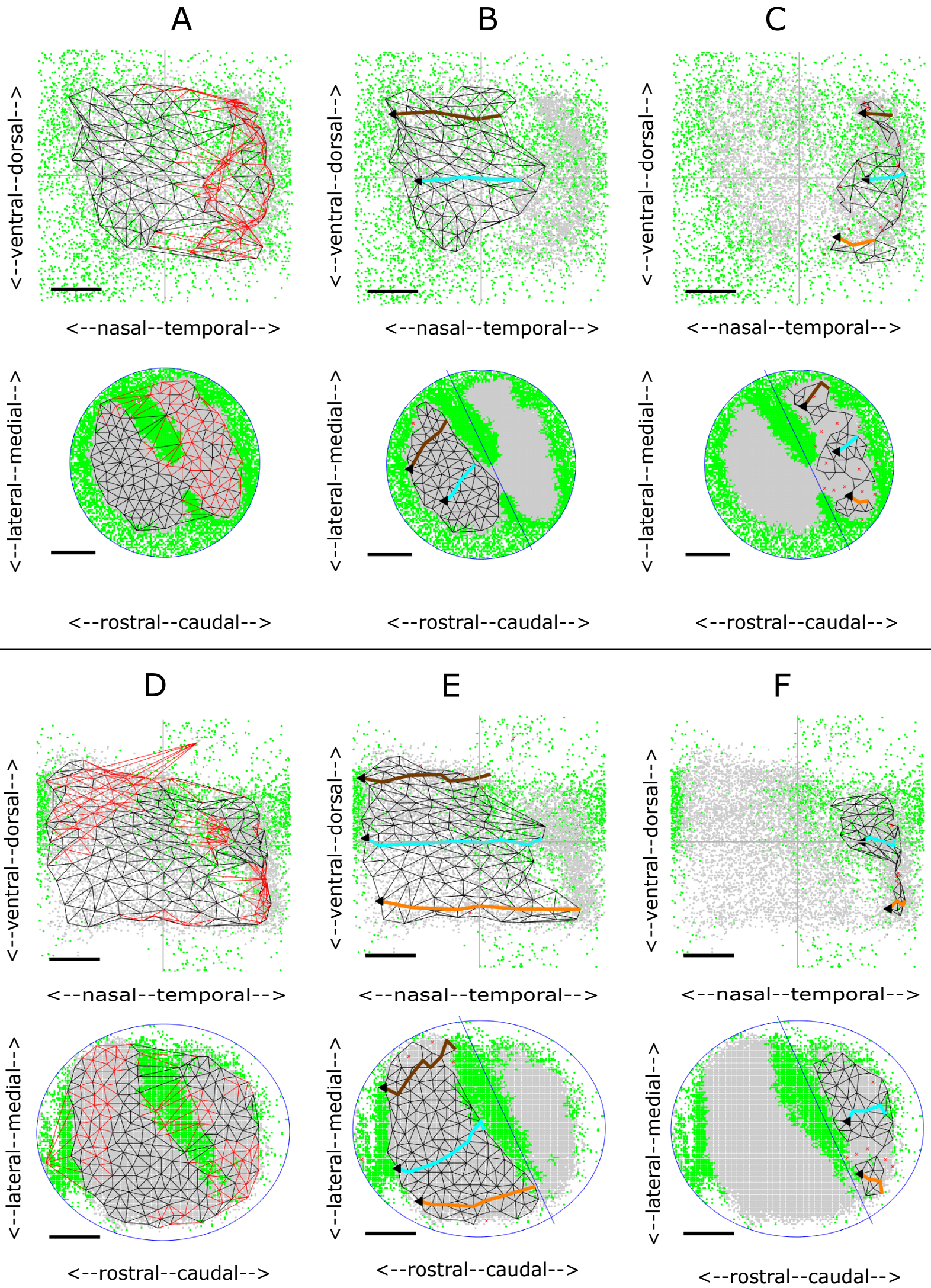
A
B
C
D
E
F
<--ventral--dorsal-->
<--nasal--temporal-->
<--lateral--medial-->
<--rostral--caudal-->

# FIGURE 4

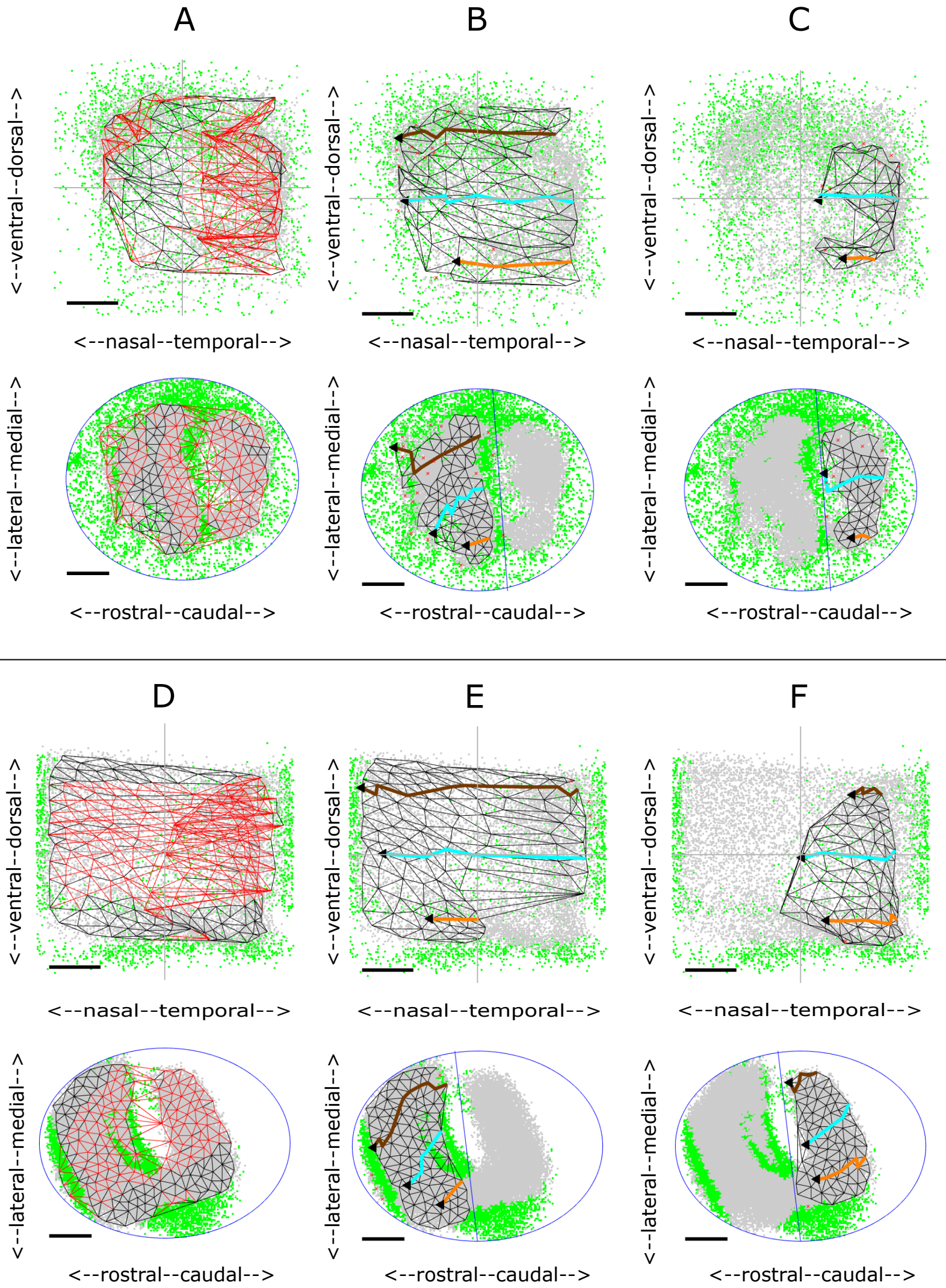
A
B
C
D
E
F
<--ventral--dorsal-->
<--nasal--temporal-->
<--lateral--medial-->
<--rostral--caudal-->

# FIGURE 5

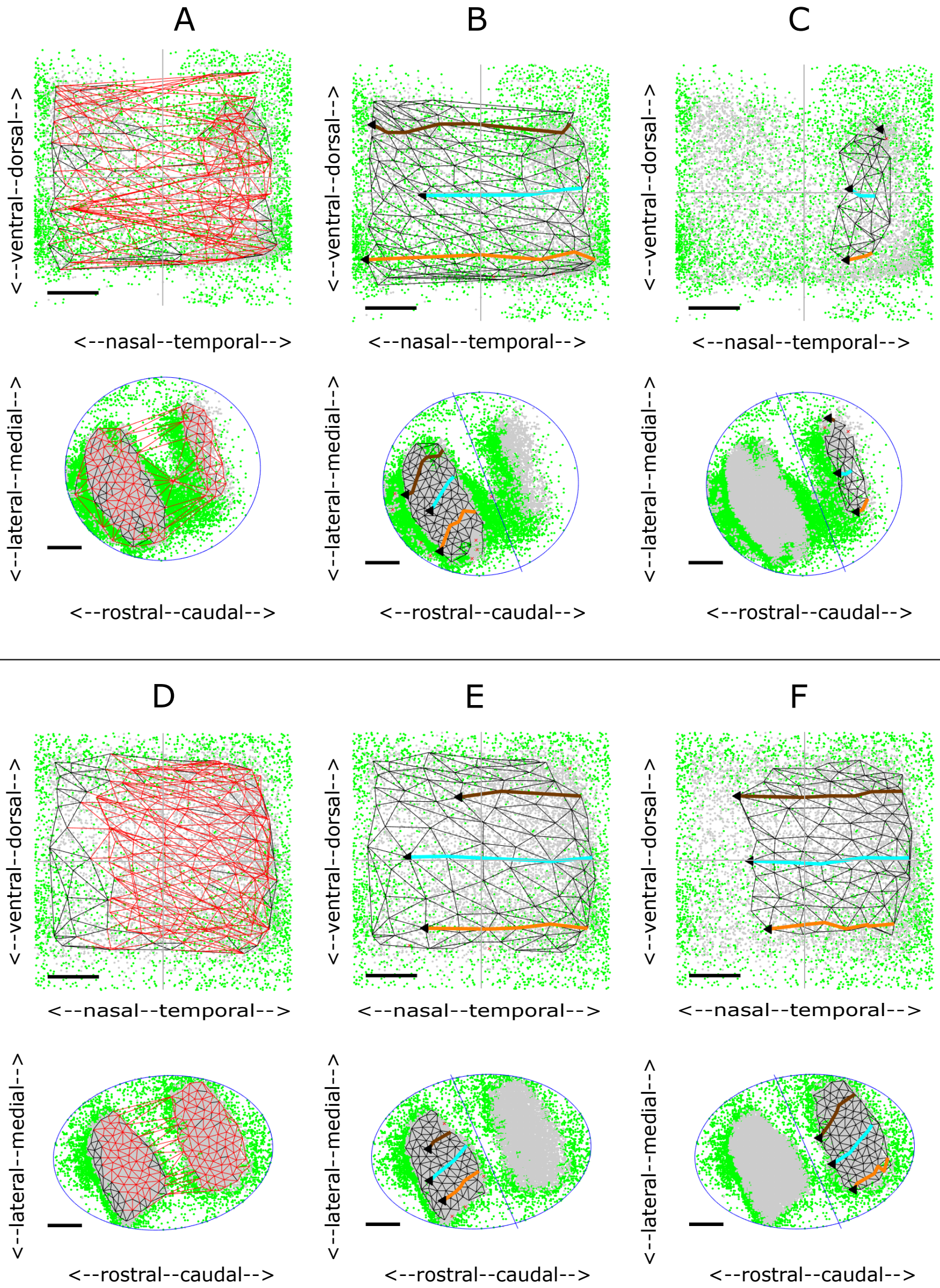
A
B
C
D
E
F
<--ventral--dorsal-->
<--nasal--temporal-->
<--lateral--medial-->
<--rostral--caudal-->

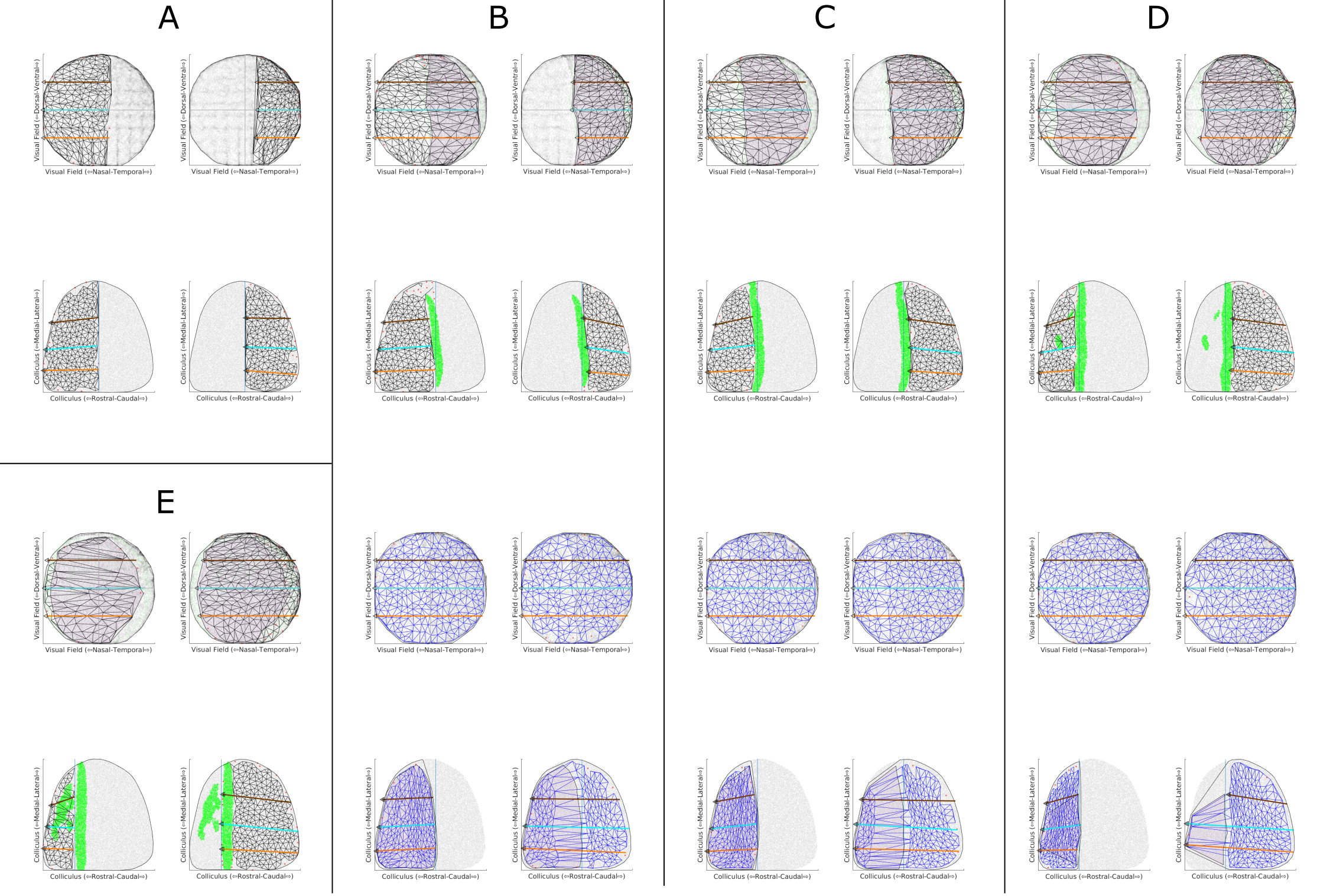
A
B
C
D
E
Visual Field (⇦Dorsal-Ventral⇨)
Visual Field (⇦Nasal-Temporal⇨)
Colliculus (⇦Medial-Lateral⇨)
Colliculus (⇦Rostral-Caudal⇨)

**FIGURE 6**

# FIGURE 7

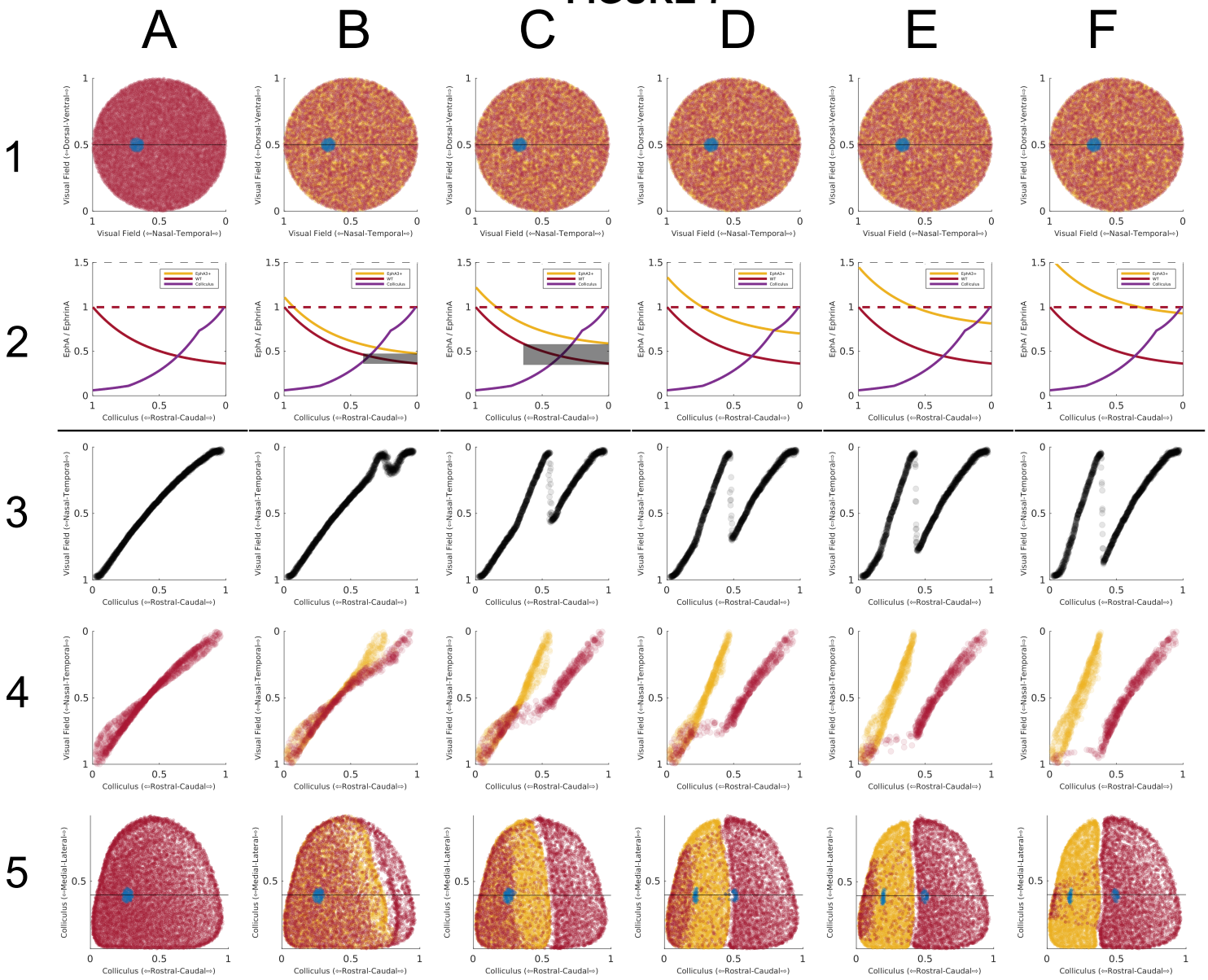
A
B
C
D
E
F
1
2
3
4
5
Visual Field (⇐Dorsal-Ventral⇒)
Visual Field (⇐Nasal-Temporal⇒)
EphA / EphrinA
Colliculus (⇐Rostral-Caudal⇒)
EphA3+
WT
Colliculus
Visual Field (⇐Nasal-Temporal⇒)
Colliculus (⇐Medial-Lateral⇒)

# FIGURE 8

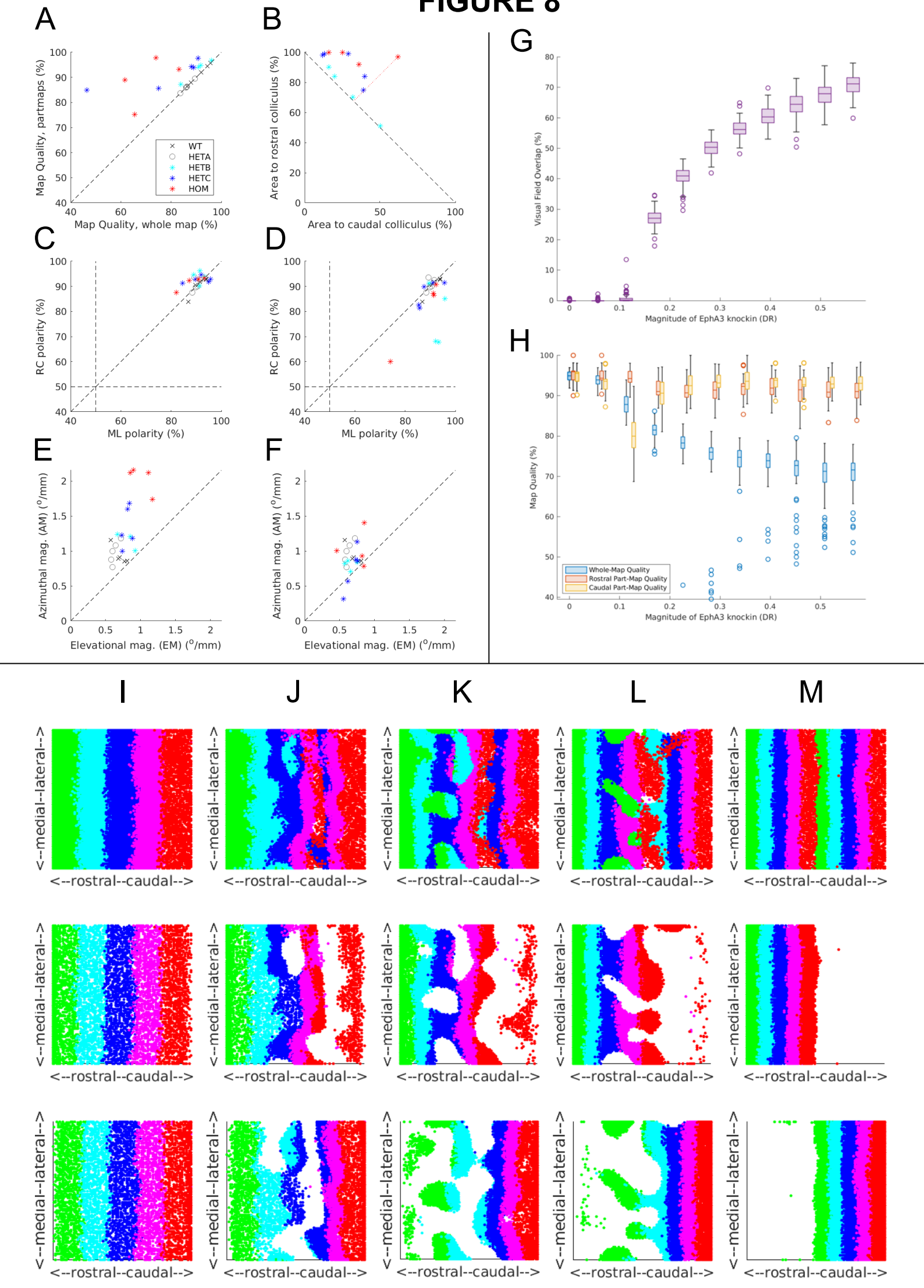
A
Map Quality, partmaps (%)
Map Quality, whole map (%)
WT
HETA
HETB
HETC
HOM
B
Area to rostral colliculus (%)
Area to caudal colliculus (%)
C
RC polarity (%)
ML polarity (%)
D
RC polarity (%)
ML polarity (%)
E
Azimuthal mag. (AM) (°/mm)
Elevational mag. (EM) (°/mm)
F
Azimuthal mag. (AM) (°/mm)
Elevational mag. (EM) (°/mm)
G
Visual Field Overlap (%)
Magnitude of EphA3 knockin (DR)
H
Map Quality (%)
Whole-Map Quality
Rostral Part-Map Quality
Caudal Part-Map Quality
Magnitude of EphA3 knockin (DR)
I
J
K
L
M
<--medial--lateral-->
<--rostral--caudal-->